Astron. Astrophys. 339, 95–112 (1998)

ASTRONOMY AND ASTROPHYSICS

The dynamic decay of young few-body stellar systems

I. The effect of a mass spectrum for N = 3, 4, and 5

Michael F. Sterzik[1,2] **and Richard H. Durisen**[2,3]

[1] European Southern Observatory, Alonso de Cordova 3107, Vitacura, Casilla 19001, Santiago 19, Chile
[2] Max-Planck-Institut für Extraterrestrische Physik, D-85740 Garching bei München, Germany
[3] Department of Astronomy, SW319, Indiana University, Bloomington, Indiana 47405, USA

Received 2 July 1998 / Accepted 12 August 1998

Abstract. We investigate the dynamic decay of nonhierarchical few-body systems, with an emphasis on applications to young stellar multiples formed by fragmenting cloud collapse. A chain regularization scheme is used to integrate orbits for 300 or more crossing times in order to guarantee that most systems are fully decayed. In this paper, we consider cases where the number N of point-mass stars is three, four, or five; and we explore effects of the stellar mass spectrum on the outcome in the low angular momentum limit. A novel classification scheme is introduced to identify the remnant decay products, including singles, binaries, and bound hierarchical multiples. The ensemble of final system configurations is then analysed to determine mass and escape speed distributions, and to characterize properties of the binary and triple stars formed during the decay. Some statistical features of the endstates can be understood analytically using well-known principles of few-body dynamics. Our results suggest observable signatures in and around star forming regions which would be expected if multiply fragmenting collapse is a common mode of star formation.

Key words: methods: statistical – celestial mechanics, stellar dynamics – stars: binaries: general – stars: formation – stars: kinematics – stars: pre-main-sequence

1. Introduction

Although many basic principles of few-body dynamics were established by the mid-1970's, there are two major reasons for revisiting the problem. First, in the context of point-mass dynamics, the complete decay of nonhierarchical few-body systems with $N > 3$ has not been studied in a comprehensive and definitive way using modern integration schemes. Second, in the context of star formation, it is clear that molecular cloud core collapse leads to multiple fragmentation under a wide variety of conditions. Understanding the relationship between molecular cloud conditions and the final multiplicity distribution of stars produced by a star forming region (SFR) requires that we know how post-collapse protostellar fragment clusters evolve. These two considerations provide the impetus for our work. Because this is the first paper in a series on this topic, we discuss the motivations in some detail.

Send offprint requests to: Michael F. Sterzik, (msterzik@eso.org)

1.1. Classic work

The decay of few-body systems is a classic problem in numerical astrophysics. One question addressed early by van Albada (1968a, b) is the formation of double stars through the disintegration of small groups. Already in this work, van Albada presented the hypothesis that small star clusters with diameters $\approx$ 100–1000 A.U. which result from fragmentation during star formation could account for the observed properties of binary stars through their subsequent decay. Several authors focused on the three-body problem (e.g., Anosova 1969, Szebehely 1972) and developed various "escape criteria" to determine when one star becomes unbound. Standish (1972) followed the dynamical evolution of triple stars and determined distributions of several quantities of astrophysical interest like times of disintegration, velocities and masses of escapers, and the semi-major axes and eccentricities of the remnant binaries. Significant insight into the decay process was gained by theoretical analyses of three-body encounters (Heggie 1975) and by a statistical theory for three-body disruption (Monaghan 1976a, b). Quantitative comparisons with numerical results of the same vintage yielded satisfactionary agreement with regard to escape velocities and final binary energies and eccentricities (Saslaw et al. 1974, Valtonen 1976). The importance of the initial system total energy was recognized early, but the system angular momentum can also be important (e.g., Standish 1972, Monaghan 1976b, Mikkola & Valtonen 1986). In order to understand the production and abundance of triple stars through few-body decay, Harrington (1974, 1975) also performed a limited number of numerical experiments for $N = 4$ and 5.

The general behavior of decaying few-body systems, as characterized by the end of the 1970's, includes the following:

– The characterisitic system lifetime is on the order of tens of crossing times.

- Encounters between stars redistribute energy in such a way that some stars escape and leave behind a more tightly bound subsystem, usually a binary.
- The remnant binary generally consists of the two most massive stars of the initial system, an effect called "dynamical biasing". The escaping single stars are generally the least massive ones.
- Tightly-bound binaries are rare. Spectroscopic binaries are difficult to explain by few-body decay.
- Stability of higher-order systems is generally achieved by hierarchical organization.
- Outcomes of numerical experiments are roughly consistent with the analytic work of Heggie and Monaghan.

The three-body problem has been revisited in the 1980's and 90's with modern computer codes, but with more of an emphasis on scattering problems than system decay (see reviews by Anosova & Kirsanov 1991 and Valtonen & Mikkola 1991; see also McMillan & Hut 1996 and earlier papers in the same series). Sophisticated orbit integration techniques permit precise treatment of frequent close encounters during the evolution of triple systems. A statistical approach is generally used to investigate the fate of systems which span a range of the initial phase space. There has been considerable modern work on the stability of planar and three-dimensional three-body systems (e.g., Black 1982, Anosova & Orlov 1994, Anosova et al. 1994, Kiseleva et al. 1994a, b, Eggleton & Kiseleva 1995). Some more specific initial configurations have been considered in great detail, such as the Pythagorean three-body problem (Aarseth et al. 1994a, b). However, modern orbit integrators have not yet been used for a thorough characterization of the complete decay for small-N clusters, including escape speed distributions and internal structures of all remnant subsystems.

1.2. Fragmentation calculations

As van Albada foresaw, it is now widely accepted, through results of hydrodynamics calculations, that fragmentation during molecular cloud core collapse is the initial step in the production of binary and multiple stars, at least for systems with large separations (see reviews by Boss 1988, Bodenheimer et al. 1993, Bodenheimer 1995, Burkert et al. 1998). For a wide range of conditions, isothermal cloud collapse is likely to produce more than two fragments. Although an important caveat has been given recently regarding numerical resolution in fragmentation calculations (Truelove et al. 1997, 1998), it is still clear that multiple fragmentation, with fragment numbers of two to five or more, is a likely outcome of protostellar cloud collapse (Bate & Burkert 1997, Burkert et al. 1997). Resulting nonhierarchical fragment configurations are quite varied and include, for instance, rings (Monaghan & Lattanzio 1991), thin strings or filaments (Bonnell et al. 1992, Boss 1993, Burkert & Bodenheimer 1993, Monaghan 1994), and cold thin disks (Boss 1996).

For reasons of computational cost, most collapse calculations are terminated once dense fragments containing only a few percent of the cloud mass have formed. Modern computational techniques have so far permitted only very few well-resolved calculations to be carried through to almost complete accretion of the cloud mass onto the fragments (e.g., Burkert & Bodenheimer 1996, Burkert et al. 1998). Burkert et al. (1998) describe the fragment evolution as "chaotic", involving successive stages of fragment formation and merger. This results in a multiple system at the end of the cloud accretion phase with essentially unpredictable and hence, to some degree, randomized orbital parameters. These collapse calculations demonstrate the formation of nonhierarchical multiple systems, and they provide the necessary step of mapping from interstellar cloud conditions on the 0.01 pc scale to fragment systems with typical scales of order 100 A.U. The parameter space of possible initial cloud states is still too vast for a proper computational characterization of collapse endstates, but it is clear that a wide range of N and of spatial and orbital configurations is possible. Once accretion ends, nonhierarchical stellar multiples will decay. It is this second stage of star formation that is the focus of our work – the mapping of young few-body systems through dynamical decay into stable and long-lived stellar remnants, such as single stars, binaries, and hierarchical multiples. As we will show, this second mapping involves another, fairly well-defined decrease in system scale.

1.3. Observational motivation

Significant information has now accumulated on the multiplicity fractions and binary orbit separations for low-mass stars in the solar neighborhood (Duquennoy & Mayor 1991, Fischer & Marcy 1992, hereafter DM and FM, respectively) and for young stellar objects and pre-main sequence stars in nearby SFR's (as reviewed by Mathieu 1994). The DM binary period distribution for solar-type stars is extremely broad. Recent observations suggest that binary frequencies (BF's) vary significantly among SFR's (Ghez et al. 1992, Leinert et al. 1992, Prosser et al. 1994, Padgett et al. 1997, Petr et al. 1998) and that the width of the separation distribution may be much narrower in individual SFR's than the DM distribution (Brandner & Köhler 1998). The DM distribution may thus be a blend of many narrower separation distributions contributed by different SFR's. There is some indication that the stellar density in SFR's anticorrelates with the observed BF (e.g., Reipurth & Zinnecker 1993, Bouvier et al. 1997, Petr et al. 1998). Two plausible mechanisms have so far been put forward for these differences: the disruption of primordial soft binaries in star clusters (Kroupa 1995) and an intrinsically lower parameter space available for (wide) binary formation in a higher temperature ambient cloud (Durisen & Sterzik 1994).

Both mappings of scale in van Albada's two-step scenario (cloud $\rightarrow$ fragment system $\rightarrow$ stellar remnants) need to be characterized in order to develop a theoretical explanation for observed binary and multiple star properties. An attempt to clarify the second process was made by McDonald & Clarke (1993) by using van Albada's analytic statistical approach. They assumed that all clusters produced exactly one binary consisting of the first and second-most massive stars of the original system, rather

than perform direct orbit integrations. In a subsequent study, they found that they could match the observed binary mass-ratio distribution and binary fractions when system stars were chosen randomly from an IMF, but only if dissipative encounters were included (McDonald & Clarke 1995). Recently, Valtonen (1997, 1998) found fairly good agreement with mass-ratio distributions for wide binaries and multiple stars using Monaghan's (1976a, 1977) statistical theory of three-body disruption.

The kinematics of young stars may also be affected by the dynamics of few-body fragment clusters. It is generally believed that young, low-mass stars diffuse away from their SFR with velocity dispersions ~ 2 to 3 km/s (e.g., Jones & Herbig 1979, Hartmann et al. 1991), comparable to the external dispersion velocities of their parental cloud cores. We were originally motivated to consider the possibility of ejecting T Tauri stars (TTS) from their SFR's at higher speeds via few-body dynamics (Sterzik & Durisen 1995, hereafter SD) by the observation that young stars identified in the ROSAT All-Sky Survey (RASS) and confirmed by follow-up optical studies are widely distributed in space around all nearby SFR's examined (Sterzik et al. 1995, Neuhäuser et al. 1995, Alcala et al. 1995, Magazzu et al. 1997, Neuhäuser et al. 1997, Alcala et al. 1997, Covino et al. 1997; for a recent review see Neuhäuser 1997). There are also a number of young stars in the immediate solar neighborhood, far from any site of recent star formation (Sterzik & Schmitt 1997, Soderblom et al. 1998) and a few cases where known kinematics suggest a relatively high-speed ejection (e.g., Neuhäuser et al. 1998). SD concluded that, while such "RATTS" (run-away T Tauri stars) were a likely consequence of few-body decay after multiple fragmentation, dynamic ejection could not explain the large number of "halo" TTS. It now seems likely that the widely distributed young RASS-selected stars represent a Gould Belt population (Sterzik et al. 1998, Guillout et al. 1998). Nevertheless, if multiply fragmenting collapse is a common mode of star formation, then few-body decay dynamics will necessarily have an effect on the kinematics of the young stars and stellar remnants that result.

Formation of stars within larger groups of hundreds to thousands of stars seems to be common (Lada et al. 1991). This can be thought of as a higher level in a hierarchy of star formation and does not preclude the formation of few-body systems through the collapse and fragmentation of subcomponents of larger groups. So, our work is complementary to that of Kroupa (1995, 1998), who has been studying the dynamics of young aggregates with larger numbers of stars ($N > 100$). Kroupa computes the kinematics and binary properties resulting from the dissolution of such aggregates for various stellar densities and velocities. The inclusion of primordial binaries enhances the proportion of high-velocity escapers. If few-body decay also occurs, it will influence the results through kinetic energy input by the decay remnants and through the presence of "primordial" multiple remnants.

1.4. Goals

Unfortunately, a clean separation between the phase of cloud gas accretion after fragment formation and the stellar dynamic evolution of the fragment system is probably not really possible. Significant accretion onto the fragments may continue for $\sim 10^4 - 10^5$ yrs, which is also an important time interval for orbital evolution. Orbit integrations with continuing accretion (e.g., Bonnell et al. 1997) are desirable but are difficult to do accurately and realisitically for more than a few realizations of possible systems. The disks likely to be present around the stars during the early stellar dynamic phase will also affect the outcome (Clark & Pringle 1991, 1993, McDonald & Clarke 1995) through disk/disk and star/disk interactions, but again it is difficult to study more than a few representations of realistic systems. The philosophy of our own work is to begin with an idealized separation of the two stages and avail ourselves of powerful modern techniques for the computation of pure few-body dynamics. A particular emphasis is identifying features of the endstate distributions which are relatively robust and independent of physical assumptions. From this point of view, it makes sense to begin with a thorough investigation of initially gas-free few-body systems and work systematically toward the inclusion of more physical effects and greater complexity in the calculations.

In SD, we developed a way to generate initial conditions for few-body orbit integrations that mimicked various plausible fragment distributions (velocity fields and geometries) and system sizes seen in cloud collapse calculations. SD then studied only the first single stars detected to be escaping from such systems ("first escapers"). We now set the more ambitious goal of determining the full dynamic decay of few-body systems, starting with relatively well-understood cases and moving systematically toward more realistic conditions. Our aim is to characterize statistically the decay channels, remnant escape speeds, and the internal characteristics of the bound binary and multiple stellar remnants. Sect. 2 of the present paper explains the way in which we specify initial conditions and how we integrate and analyze gas-free systems. Results are presented in Sect. 3 for cold, spherical, low angular momentum $N = 3$, 4, and 5 systems with three different initial stellar mass spectra. Later papers in this series will consider the effects of distorted geometries, systematic motions, and other physics. Sect. 4 discusses applications to star formation, while Sect. 5 summarizes our main conclusions.

2. Methodology

2.1. Numerical approach

Our basic approach is to compute the orbital evolution of a large number of realizations (1,000) for various particular types of initial few-body system. The different types of system are distinguished by the total number of particles N, the assumed mass spectrum of the constituent stars, the shape of the system (spherical, prolate, or oblate), the magnitude of the particle random motions, and the magnitude and direction of any systematic

rotation. Although, procedurally, our initial few-body system realizations are in physical units, the units are transformed for integration to a dimensionless form which highlights the generality of the results. We characterize the complete decay of the few-body system by orbit integrations which are long enough so that the system has broken into a subset of spatially well-separated, long-lived remnants which are not bound to each other, which themselves are internally bound, which suffer no further close interactions with other remnants, and which are far enough apart that the gravitational interactions between them are negligible. We find that integrations over 300 initial crossing times T_{cr} suffice to converge the multiplicity fractions of remnants to within a few hundreths by intercomparing results after 100, 300, and 1,000 T_{cr} for a few cases. Of course, some of the remnants are hierarchical multiples which are metastable and will decay further on longer time scales; and some systems (usually only a few per 1,000) remain nonhierarchical and undecayed even after 1,000 T_{cr}. For applications to star formation, a few long-lived metastable configurations and rare singular outcomes are not a serious concern.

2.2. Initial conditions

For a given N, we specify the masses, geometry, and velocities of the systems by a Monte Carlo realization of 1,000 systems from a set of assumed initial distributions.

Masses. N masses M_i, $i = 1$ to N, with total mass M_{tot}, are first chosen randomly from a prescribed mass spectrum (see 2.3 below).

Geometry. The positions of the masses are then chosen randomly within an ellipsoidal volume with semi-axes $x_0 \geq y_0 \geq z_0$. For most cases in this paper, we consider "spherical" systems in the statistical sense that $x_0 = y_0 = z_0$. Effects of severe distortions in the fragment distributions, as suggested by some collapse calculations, will be explored in the next paper of this series. At this point, the total gravitational energy W of the system is computed.

Initial Velocities. Once positioned, the particles can be given randomly chosen velocity components and/or a systematic uniform rotation about a specified axis through the center of mass (COM), and the coordinates and velocities are transformed into the COM frame. Velocities are now rescaled so that the total random kinetic energy K_{rand} and the total rotational kinetic energy K_{rot} satisfy prescribed values of $\alpha = K_{rand}/|W|$ and $\beta = K_{rot}/|W|$. If desired (see Sect. 4.3), the lengths and velocities may be further rescaled so that some target system size or total energy E_0 or energy per unit mass E_0/M_{tot} is achieved, while preserving α and β. However, this has no effect on the integrations, which are done in dimensionless units. For most integrations in this paper, $\alpha = \beta = 0$, i.e., the systems are "cold" and have zero net angular momentum.

Dimensionless Units. The system is transformed to dimensionless code units by setting (Heggie & Mathieu 1986)

$$\begin{cases} G = 1 \\ M_{tot} = 1 \\ E_0 = -1/4 \end{cases} \tag{1}$$

In these units, "Hénon's virial radius" (Hénon 1972)

$$R_H = \frac{GM_{tot}{}^2}{4|E_0|} = 1. \tag{2}$$

For $N \to \infty$ and equal masses, R_H is equal to the true virial radius, defined exactly in that limit as the harmonic mean of the particle separations. R_H is a good measure of the physical size that the few-body system would have if it relaxed into virial equilibrium, and so it provides a natural reference scale for the integrations. Similarly, the "virial speed" v_{vir} and the "crossing time" T_{cr} can be defined by

$$\begin{cases} v_{vir} = (2|E_0|/M_{tot})^{1/2} = (GM_{tot}/2R_H)^{1/2} = \sqrt{2}/2 \\ T_{cr} = 2R_H/v_{vir} = (2R_H)^{3/2}/(GM_{tot})^{1/2} = 2\sqrt{2} \end{cases} \tag{3}$$

2.3. Mass spectra

Let $f(M)dM$ be the probability of choosing a star with mass M in the mass interval dM. Three choices of f are used in this paper.

Equal Masses (EM). This case is considered for two reasons. Some precise and even analytic results are available in this limit for $N = 3$. Also, it is necessary to define the base state for equal masses in order to determine which aspects of the endstate distributions are sensitive to $f(M)$ and which are not.

Miller-Scalo Power Law (MS). While the mass function for the fragment systems that result from cloud collapse is still not known, there is evidence (DM, FM) that the secondary stars in low-mass binaries are chosen randomly from the overall stellar initial mass function (IMF). So one set of calculations is done with a power-law f that represents a crudely realistic IMF for low-mass stars. The exponent is chosen to match the slope of the Miller-Scalo (1979) IMF near solar-mass stars,

$$f_{ms}(M) = \begin{cases} \text{constant} \cdot M^{-1.1} & \text{for } 0.1M_\odot \leq M \leq 10M_\odot \\ \text{zero} & \text{otherwise} \end{cases} \tag{4}$$

In dimensionless integration units, this mass spectrum is effectively tapered at the upper and lower mass cutoffs due to the M_{tot} = 1 renormalization (see Fig. 1). We distinguish distributions of dimensionless masses m from their dimensional counterparts by an asterisk, in this case $f^*_{ms}(m)$.

Clump Mass Spectrum (CM). Molecular cloud complexes are know to be clumpy on a variety of scales with a possibly fractal structure that gives a power-law clump mass spectrum with an index of about -1.5 to -2.0 (e.g., Elmegreen & Falgarone 1996). Thus the cloud cores that collapse and fragment may

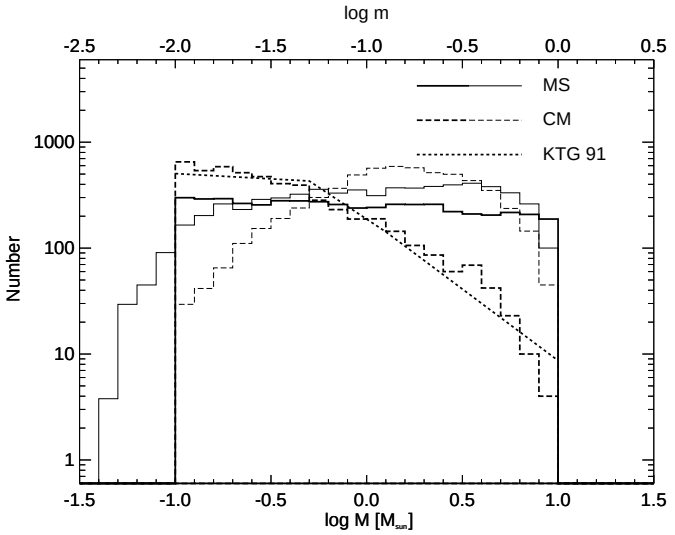

Fig. 1. The MS (solid) and CM (dashed) mass spectra for our $N = 5$ systems histogrammed in even logarithmic intervals. Heavy curves are the $f(M)$ in physical units; thin curves are the dimensionless $f^*(m)$. Shown for comparison is part of the Kroupa et al. 1991 IMF (dotted curve).

themselves have a power-law mass distribution. To mimic this case, we first choose an M_{tot} from

$$f_c(M) = \begin{cases} \text{constant} \cdot M^{-1.5} & \text{for } 0.9M_\odot \leq M \leq 10M_\odot \\ \text{zero} & \text{otherwise} \end{cases} \quad (5)$$

For each M_{tot}, we then use Eq. (4) to determine the individual stellar masses M_i subject to the constraint that the choices sum to M_{tot} to within $\pm$ 5%. We refer to the combined dimensional mass spectrum as $f_{cm}(M)$, and its nondimensional counterpart as $f^*_{cm}(m)$. Fig. 1 intercompares f and f^* for both the MS and CM mass spectra of our $N = 5$ systems. The dotted curve shows the Kroupa et al. (1991) IMF normalized to produce 5,000 stars in the mass range of Eq. (4). Our f_{cm} prescription results in a similar IMF.

2.4. Numerical integrations

For each type of few-body system, the particle orbits of all 1,000 realizations are integrated for 300 T_{cr} using the Mikkola & Aarseth (1990, 1993) chain regularization method. By guaranteeing large spatial separations of the decay remnants, these long integrations permit an unambiguous and automatic identification of the remnants themselves, a nontrivial exercise for $N \geq 4$. By minimizing residual gravitiational interactions between remnants, it also allows us to determine accurate escape speeds (the limit of infinite remnant separations), without large, ill-defined corrections. Most systems actually decay within dozens of T_{cr}; but we find it preferrable to integrate all systems for the same number of T_{cr}, rather than apply decay criteria in a time-dependent way during integration.

Unfortunately, the length of the integrations does create some difficulties. Despite the accuracy of the integration scheme, large energy errors can accumulate in systems where a high-eccentricity binary forms because it can make many thousands of close periapse passages over 300 T_{cr}. The errors usually become significant only well after the complete decay of the system has occurred. We are not interested in mapping initial and final points in phase space with high precision, but we do wish to determine binary semi-major axis distributions and the escape speeds of remnants. These distributions are affected by the distribution of final energies, so we keep the relative error in $|E_0|$ below 0.1% by the following procedure. For each type of few-body system, the initial 1,000 integrations are performed with a tolerance parameter (see Mikkola & Aarseth 1993) of 10^{-12}. After 300 T_{cr}, the E_0 errors are checked. Any system with a relative energy error $> 0.1\%$ is reintegrated for the same initial conditions with a tolerance parameter of 10^{-15}. For the worst case in this paper ($N = 5$ equal masses), no more than a few dozen reintegrations per 1,000 systems are necessary. The final energy errors are again checked. Usually, after this step, no more than a few percent ($\sim$ 10 to 30) of the systems have relative energy errors $>$ 0.1%. These systems are flagged and omitted from any further analysis which might be sensitive to energy. The vast majority of the integrations are of high quality, as demonstrated by the fact that the median relative energy error for 1,000 system integrations is typically $\sim \pm 10^{-6}$ after 300 T_{cr}.

2.5. Hierarchical virtual-particle analysis

A statistical characterization of complete few-body system decay requires the unambiguous identification of remnant subsystems at the endpoint of the integrations. For this purpose, we developed an analysis technique involving successive passes through the endstate data.

We start with the final positions and velocities of the N particles. For each pairing of the stars, we decide whether the pair is a bound binary subsystem. To be so-classified, the pair must satisfy the following two criteria: i.) In the COM of the pair considered as an isolated system, the two-body orbital energy must be negative. ii.) No other star is present within a spherical volume centered on either member of the pair with a radius equal to the major axis of the pair's relative orbit. In all cases, at this first level of the hierarchical treatment, we find that binary pairs are uniquely identified. These binaries are then treated as virtual particles for the next level of analysis. The virtual particle is given the COM velocity and position for the pair and a mass equal to the sum of the masses. Binary orbit characteristics are computed at this stage in dimensionless units and stored. If N_b binaries are identified in the first pass, there are now $N - N_b$ "particles", real stars plus binaries, in the next level of analysis. The procedure for the next pass is the same; all pairs of particles, whether representing binaries or real singles, are again checked according to the same two criteria (i) and (ii). At this level, it is possible to discover new subsystems where a binary virtual particle is found to be bound to another binary (a "binary quadruple") or to a single star. This idenitifies hierarchical triples and hierarchical pairs of binaries. The orbit

characteristics of these systems are also computed and stored. These two levels of hierarchical structure analysis suffice for $N = 3$; but, for $N = 4$ and 5, one more level is required to identify "planetary quadruples", where a hierarchical triple has a fourth component orbiting at a large distance.

There is an implicit assumption in this analysis that, after 300 T_{cr}, the substructure of the remnants will be hierarchical. If no virtual particles are found, it is assumed that the system has remained undecayed. At the end of the analysis, a self-consistency check is made to ensure that the virtual particles identified have positive kinetic energy in the system COM and that this positive kinetic energy is larger in magnitude than the absolute error in the total system energy.

Altogether the following categories of decay products are possible:

BS: binary plus $N-2$ singles
TS: triple plus $N-3$ singles
Q_pS: planetary quadruple plus $N-4$ singles
Q_bS: binary quadruple plus $N-4$ singles
BBS: two binaries plus $N-4$ singles
TB: triple plus binary
U: undecayed nonhierarchical system
E: relative energy error $> 0.1\%$

Here, single, binary, triple, and quadruple refer to independent bound remnants, which are unbound from other remnants. Triples and quadruples are understood to be hierarchical. We do not attempt to distinquish between hierarchical and non-hierarchical bound quintuples. One can think of these different categories as the "decay channels" for the few-body systems.

2.6. Analytic approach

Analytic predictions for escape speed and binary separation distributions can be made from the pioneering work of Heggie (1975). Heggie showed by approximate analytic arguments that, in the limit of low system angular momentum, the distribution of final binary energies E_b resulting from the decay of nonhierarchical bound triples should have the form

$$g_E(E_b) = 3.5|E_0|^{7/2}|E_b|^{-9/2}, \tag{6}$$

where g_E is the fraction of binaries in the interval $d|E_b|$. In various contexts, Eq. (6) is referred to as "Heggie's Law" (e.g., Valtonen & Mikkola 1991). The E_b dependence of this formula can be understood crudely as follows. A factor $|E_b|^{-5/2}$ arises simply from expressing the binary relative motion phase space in terms of orbital elements and integrating out the eccentricity and angular coordinate terms. The other factor of $|E_b|^{-2}$ reflects the energy-dependence of Σv (the cross-section times the relative velocity) for encounters that give rise to binary energies of E_b. The binaries are produced mostly by close encounters for which one expects the cross-section to vary roughly as a^2, where a is the semi-major axis of the resulting binary relative orbit given by

$$E_b = -\frac{GM_iM_j}{2a}\ , \tag{7}$$

while the encounter speed v at large distances is just v_{vir} and independent of $|E_b|$.

In the same 1975 paper, Heggie also considered the creation rate of hard binaries from soft binaries through close two-body encounters between one component of the binary and a third star in a large-N cluster. The creation rate in the interval $d|E_b|$ is then proportional to $|E_b|^{-7/2}$ due to a different energy-dependence of Σv. One might expect some binary formation events to be better described in this way, especially for $N > 3$. The binary creation and destruction rates in Heggie's 1975 paper are only approximate (e.g., Heggie & Sweatman 1991). Monaghan (1976a, b) and Nash & Monaghan (1978) took the different point of view that, statistically, the binaries formed from three-body systems would be uniformly distributed through allowed phase space by the quasi-ergodic nature of the close interactions. A simplified version of this argument, where one ignores angular momentum conservation and assumes three-dimensional systems, yields a $|E_b|^{-5/2}$ distribution based on the phase-space volume for binary orbits. Given these uncertainties, we, like other researchers in similar contexts (Mikkola & Valtonen 1986), consider a "generalized Heggie's law"

$$g_E(E_b) = (\gamma-1)|E_0|^{\gamma-1}|E_b|^{-\gamma}. \tag{8}$$

We expect γ to be in the range 5/2 to 9/2.

In the remainder of this section, we use Eq. (8) to generate analytic escape speed and binary separation distributions. Our approximate arguments result from efforts to obtain reasonable fits to our experimental results. For $N = 3$, binary formation in the BS mode is the only true decay channel, and so (8) should be directly applicable. For $N = 4$ and 5, the dominant decay channels are BS and TS, where a single close binary (either a free remnant or the smaller component of the hierarchical triple) releases the bulk of the energy that unbinds the system, and so again we expect (8) to apply.

For equal masses $m = 1/N$, the semi-major axis distribution g_a expected from Eq. (8) is

$$g_a(a) = \begin{cases} (\gamma-1)(2m^2)^{1-\gamma}a^{\gamma-2} & \text{for } a \le a_{max} \\ 0 & \text{otherwise} \end{cases} \tag{9}$$

in dimensionless units, where $g_a da$ is the fraction of BS binaries with a in the interval da and where

$$a_{max} = 2m^2. \tag{10}$$

For $N = 3$ (4, 5), $a_{max} = 2/9$ (1/8, 2/25). The maximum of (9) is at $a = a_{max}$, and the average value $\bar{a}$ is given by $\bar{a}/a_{max} = (\gamma-1)/\gamma$.

For the BS case of $N = 3$, the escape speeds of the single star v_s and of the binary v_b are completely determined from a by momentum and energy conservation as

$${v_s}^2 = 4{v_b}^2 = \frac{1}{3m}\left(\frac{2m^2}{a} - 1\right). \tag{11}$$

One consequence of momentum conservation is that the single star has exactly two-thirds of the final kinetic energy that unbinds the sytem. Using Eq. (9), we can then write the escape speed distributions for singles g_s and binaries g_b as

$$g_s(v_s) = 6(\gamma-1)mv_s(1+3mv_s^2)^{-\gamma} \tag{12}$$

and

$$g_b(v_b) = 2g_s(2v_b), \tag{13}$$

where $g_s dv_s$ and $g_b dv_b$ are the fractions of singles and binaries in the intervals dv_s and dv_b, respectively.

For $N = 4$ and 5, there is more freedom in dividing momentum and energy among the remnants. Suppose that, overall, the energy available to the singles is shared by them equally; but otherwise the relative kinetic energy share of the singles is still, on average, about two-thirds. Then,

$$g_s(v_s) \approx 6(\gamma-1)m\bar{n}_s v_s(1+3m\bar{n}_s v_s^2)^{-\gamma}, \tag{14}$$

where $\bar{n}_s$ is the average number of single escapers per single-emiting decay. By analogy to the momentum argument ($v_b = m_s v_s/m_b$) that applies exactly only for the three-body case, we can generalize (14) to all remnant types as

$$g_\mu(v_\mu) \approx 2(\gamma-1)A_\mu^e v_\mu(1+A_\mu^e v_\mu^2)^{-\gamma}, \tag{15}$$

where

$$A_\mu^e = 3\bar{m}_\mu^2\bar{n}_\mu/\bar{m}_s. \tag{16}$$

The subscript μ here refers to the multiplicity of the remnant (single, binary, triple, or quadruple), m_μ is the mass for remnant type μ, $\bar{n}_\mu$ is the average number of remnants of multiplicity μ per decay that produces a remnant of that type, and superscript e refers to equal masses.

There is an important difference in the final kinetic energy distribution for the case of very unequal masses with any N, because the single escapers tend to be much less massive than the binaries and multiples. As a result, the single escapers tend to carry off almost all the kinetic energy that unbinds the system. So, for unequal masses,

$$g_\mu(v_\mu) \approx 2(\gamma-1)A_\mu^u v_\mu(1+A_\mu^u v_\mu^2)^{-\gamma}, \tag{17}$$

where

$$A_\mu^u = 2\bar{m}_\mu^2\bar{n}_\mu/\bar{m}_s \tag{18}$$

and $\bar{m}_\mu$ is now the ensemble average mass for remnants of multiplicity μ. To make the dependence on basic system parameters more evident, we note that, when we do not introduce $E_0 = -1/4$ in Eq. (8), the only change in (17) and (18) is that

$$A_\mu^u = \bar{m}_\mu^2\bar{n}_\mu/2\bar{m}_s|E_0|. \tag{19}$$

(see Eq. [7] of Saslaw et al. 1974).

Table 1. Decay channel distribution.

N	f	BS	TS	Q$_p$S	Q$_b$S	BBS	TB	U	E
3	EM	832	163					1	4
	CM	874	118					1	7
	MS	878	103					1	18
4	EM	635	208	70	18	59		3	7
	CM	751	181	29	8	12		1	18
	MS	770	163	24	5	10		1	27
5	EM	415	247	117	12	121	24	23	41
	CM	532	340	53	9	41	8	6	11
	MS	588	304	32	1	31	8	2	34

We now generalize g_a in (9) to the case of a mass spectrum. Replace m^2 in (9) by $m_{ij} = m_i m_j$, the dimensionless product of the masses in a binary remnant, and assume that (9) applies with the same γ for every possible value of m_{ij}. Then, the full separation distribution can be constructed by folding together (9) and the distribution $g_{ij}(m_{ij})$ of binary mass products, where $g_{ij}dm_{ij}$ gives the fraction of binary remnants in dm_{ij}. We get

$$G_a(a) \approx \frac{\gamma-1}{2}\left(\frac{a}{2}\right)^{\gamma-2}\int_{a/2}^{1/4}\frac{g_{ij}}{m_{ij}^{\gamma-1}}\,dm_{ij}, \tag{20}$$

where $G_a da$ is the fraction of binaries in da.

3. Numerical results

3.1. General

Before we discuss the results for each system type in more detail, we summarize information that allows a statistical comparison of the outcomes. All cases are cold ($\alpha = 0$), nonrotating ($\beta = 0$), and spherical ($x_0 = y_0 = z_0$) and are distinguished only by the choice of N and f.

Decay Channels. Table 1 gives the absolute number of systems found in each decay channel (see Sect. 2.5) after our typical integration time of 300 T_{cr}. Summing over all decay channels results in the 1,000 systems that we started with, and so the statistical significance of the numbers can be gauged directly. Of course, more decay channels are accessible for larger N. We note the following general trends:

- The dominant decay mode is BS = one binary plus $N-2$ singles; but TS, Q$_p$S, and BBS are not negligible when allowed.
- For a fixed mass spectrum, larger N increases the number of higher multiplicity remnants (hierarchical triples and quadruples) in the endstates.
- The broader f^* (EM→CM→MS, see Fig. 1), the higher the relative fraction of BS endstates compared with channels that have higher multiplicity remnants.

Multiplicity Fractions. Using the above numbers, we can derive the overall fractions of remnant singles, binaries, triples, and higher-order systems. For easy comparison with observational work, we define the multiplicity fraction as the total number of

Table 2. Multiplicity fractions.

N	f	total	SF	BF	TF	QF	UF+EF
	EM	1832	.454	.454	.089		.003
3	CM	1874	.466	.466	.063		.004
	MS	1878	.468	.468	.055		.010
	EM	2537	.583	.297	.082	.035	.004
4	CM	2695	.624	.288	.067	.014	.007
	MS	2713	.627	.291	.060	.011	.010
	EM	3144	.633	.217	.086	.041	.024
5	CM	3428	.694	.181	.102	.018	.005
	MS	3475	.701	.189	.090	.009	.010

Table 3. One-dimensional velocity dispersion σ.

N	f	σ(S)	σ(B)	σ(T)
	EM	0.50	0.25	0.00
3	CM	1.08	0.14	0.00
	MS	1.32	0.13	0.00
	EM	0.43	0.27	0.14
4	CM	0.75	0.17	0.12
	MS	0.87	0.15	0.11
	EM	0.39	0.26	0.15
5	CM	0.70	0.21	0.13
	MS	0.80	0.17	0.12

each remnant type divided by the total number of remnants of all types. This definition of binary frequency BF is compatible with that of DM and others (e.g., Köhler & Leinert, 1998) who define the BF as the number of secondaries per 100 sample stars. In addition to a BF, we define in a similar fashion a single-star frequency SF, a triple frequency TF, etc. In Table 2 we give these fractions, in addition to the total number of remnants ("total") of all types. This table is constructed from the information given in Table 1 by totaling the number of remnants of different types. Remarkably, the influence of the assumed $f(M)$ on the multiplicity fractions is much weaker than it is for the distribution of outcomes over decay channels. The multiplicity fractions are dominated by the influence of N. As a measure of the importance of higher-order remnants, consider that, if every decay followed the BS channel, we would get a BF of 0.5 (0.33, 0.25) for N = 3 (4, 5). The relative deviation from this pure-BS value increases with increasing N.

Velocity Dispersions. In Table 3, we give the one-dimensional dispersions for the endstate velocities of singles (S), binaries (B), and triples (T) as measured by the standard deviation σ in the one-dimensional velocity distributions. The σ's from the three independent velocity components have been averaged together. Two dominant effects are readily identified:

- The velocity dispersions are most strongly affected by the shape of $f(M)$. The broader f^*, the more low-mass single escapers there are with relatively high velocities.
- Smaller N-body systems give higher dispersion velocities for single escapers. Comparing $N = 3$ and $N = 5$ one finds a relative difference in σ of 20–50%, in agreement with SD for first single-star escapers.

Table 4. Dynamical biasing in binary systems.

N	f	m_1m_2	m_1m_3	m_2m_3
3	CM	0.80	0.19	0.01
	MS	0.82	0.16	0.02
4	CM	0.81	0.15	0.03
	MS	0.86	0.12	0.02
5	CM	0.81	0.15	0.04
	MS	0.90	0.09	0.01

Dynamical Biasing. It is well known that binaries formed through dynamical capture within disintegrating small-N clusters preferentially consist of the first and second-most massive stars. Let us order the stars in our systems so that m_1 is the most massive, m_2 the second-most massive, and so on. The assumptions that all decays are BS and that all binaries actually consist of m_1 and m_2 enables one to derive analytic binary mass-ratio distributions for a specified f (van Albada 1968a, McDonald & Clarke 1993). For $N = 3$, Monaghan's statistical theory predicts deviations from this assumption of pure dynamical biasing. In Table 4, we assess the magnitude of these deviations in our own data by giving the fractions of all binary remnants built up from m_1, m_2, and m_3. For $N > 3$, pairings with even lower-mass components are possible, but rare. Deviations from pure dynamical biasing are in the range of 10–20%. There is a tendency for dynamical biasing to strengthen as N increases and f^* broadens.

3.2. Length of integration

For star formation, the mapping discussed in SD from pre-collapse cloud conditions to the size of the initial N-body system gives $T_{cr} \sim 300$ yrs (for $M_{tot} = 3M_\odot$ and $R_H = 125$ A.U., see Sect. 4.3). So, beyond 1,000 T_{cr}, we compromise the applicability of our results to star formation. Narrowing the choice of our standard integration time to 300 T_{cr} is then a compromise between good statistical characterization of the endstates and the quality (and computational cost) of the integrations.

Table 5 shows multiplicity fractions for the equal mass case after 100, 300, and 1,000 T_{cr}. For each N, the same set of 1,000 initial conditions was used. The meanings of the various fractions is the same as in Table 2, except that here we include the systems with large energy errors in the multiplicities. As discussed in Sect. 2.4, the energy errors usually occur well after decay within high-eccentricity remnant binaries. We exclude these systems from other analyses because we are interested in energy distributions. Here, however, they must be retained in order to determine how quickly the fractions of various remnant types converge. As shown in the last column of the table, the number E of systems with bad energies increases steadily with integration time. It is clear from $N = 5$ that we need to adopt an integration time considerably less than 1,000 T_{cr}.

On the other hand, Table 5 illustrates that there are significant numbers of remnants with high multiplicity which take many hundreds of T_{cr} to decay. Note, for instance, the TF column for $N = 3$ and the QF column for $N = 4$ and 5. Delayed

Table 5. Time evolution of the multiplicity fractions for equal masses.

N	T_{cr}	total	SF	BF	TF	QF	UF	E
	100	1646	.392	.392	.202		.013	
3	300	1835	.455	.455	.089		$<$.001	4
	1000	1919	.479	.479	.042		$<$.001	6
	100	2427	.562	.279	.087	.068	.004	4
4	300	2544	.584	.296	.084	.035	.001	7
	1000	2607	.591	.306	.082	.021	$<$.001	27
	100	3096	.634	.206	.089	.054	.017	17
5	300	3207	.642	.216	.090	.043	.008	41
	1000	3294	.649	.225	.092	.027	.007	91

Table 6. EK triple stability criterion for equal masses (energy errors $< 0.1\%$).

N	100 T_{cr}	300 T_{cr}	1000 T_{cr}
3	330(152)	163(48)	79(13)
4	205(99)	208(70)	201(52)
5	273(91)	271(65)	259(46)

decay of these systems boosts the SF and BF fractions with integration time. It is generally true, however, that the remnant fractions for the lower multiplicity types have converged to within ± 0.01 or so by 1,000 T_{cr} and that the reservoir of higher multiplicity systems is insufficent to change these numbers by much more than this amount in subsequent times. At 300 T_{cr}, with the exception of the particularly difficult case of $N = 3$ equal masses, the fractions for remnants of lower multiplicity do not differ from those at 1,000 T_{cr} by more than about 0.01. So, the convergence by 300 T_{cr} is good to within a few 0.01's or better. Furthermore, by stopping at 300 T_{cr}, we keep the additional uncertainty due to rejection of the E systems at the same order or less. The uncertainties caused by a finite integration time are not too different from the intrinsic statistical errors caused by having only 1,000 system realizations, and so a larger number of integrations would not significantly improve our results.

Another measure of the completeness of our few-body system decays is the longevity of the resulting multiple remnants. Eggleton & Kiseleva (1995, hereafter EK) developed a relatively simple analytic criterion for the stability of hierarchical triple systems through fits to a large number of orbit integration results. Their criterion gives an approximate critical value for the ratio of outer to inner orbit periods below which a triple is "two-unstable", i.e., changes its hierarchical structure, usually by decay, within 10^2 outer orbit periods. The critical period ratio depends only on the mass ratios and orbit eccentricities, which we know from our virtual-particle analysis.

Table 6 gives the total number of hierarchical triple remnants for equal mass systems at different times. In parentheses is the number of those triples that are "two-unstable" according to EK. Clearly we do not follow all these systems for 10^2 outer orbit periods; but we do expect that the bulk of the triples that do decay should be those satisfying the EK criterion, as borne out by the table. The interpretation is complicated by several factors. The first is that, for $N = 4$ and 5, the number of triples is replenished somewhat over time by the decay of higher-order systems. Nevertheless, there is convergence toward having mostly two-stable hierarchical triple remnants. The second complication is that, for all N, our zero angular momentum initial conditions create a relatively large number of systems with inner and outer orbit eccentricities $e > 0.9$. EK only test their criterion for $e \leq 0.9$. Moreover, in this context, "unstable" only means that the system changes its hierarchical structure; it does not necessarily imply that the system will decay. For unequal masses, similar tests give stronger results, where by 1,000 T_{cr} there are relatively few triples left which are two-unstable by the EK criterion.

Table 7. Comparison with other $N = 3$ results for equal masses.

author	systems	decay	$\bar{e}$	$\bar{a}$
AO	1,000	84.8%	0.705	0.170
AOA	2,500	-	0.724	0.187
this work	1,000	83.2%	0.715	0.152

For the rest of this paper, all our experimental results are quoted for 300 T_{cr}, unless otherwise noted.

3.3. Equal masses

3.3.1. $N = 3$

The case of $N = 3$ equal masses provides comparisons with other work and the tightest constraints on the development of analytic fits. Two sets of integrations with different modern codes are discussed in Anasova & Orlov (1994, hereafter AO) and Anasova et al. (1994, hereafter AOA). Due to the different technical emphases of these researchers, however, there are only a few parameters available for us to compare. As shown in Table 7, our results for the average values of the final binary e and a agree about as well with AO and AOA as AO and AOA agree with each other. For AO, the precentage of systems decaying into a binary plus unbound single is determined by various "escape criteria". Our percentage decay, given at 300 T_{cr}, is based on virtual-particle analysis. In fact, by 1,000 T_{cr}, we find that more like 92.1% of the three-body systems have decayed. Of the three codes, we would expect our Mikkola & Aarseth chain regularization scheme to be best for treating the close three-body encounters responsible for smaller values of a; and this may be responsible for our lower value of $\bar{a}$. Overall, the differences in Table 6 are acceptable for describing the effects of few-body dynamics on star formation.

The energetics of the resulting remnants are determined by the binary energy distribution g_E. Sect. 2.6 outlined arguments for $\gamma = 5/2$, 7/2, or 9/2 in the analytic g_E (Eq. [8]). Rather than use some statistical measure which might build in subtle biases, we determine the overall quality of fit by eye in plots of g_E, g_s, and g_a and limit ourselves to selecting only one of the three discrete values of γ for each N and f. Fig. 2 compares our experimental g_E with these power-law distributions normalized to produce the same number of binaries. We clearly favor $\gamma = 7/2$.

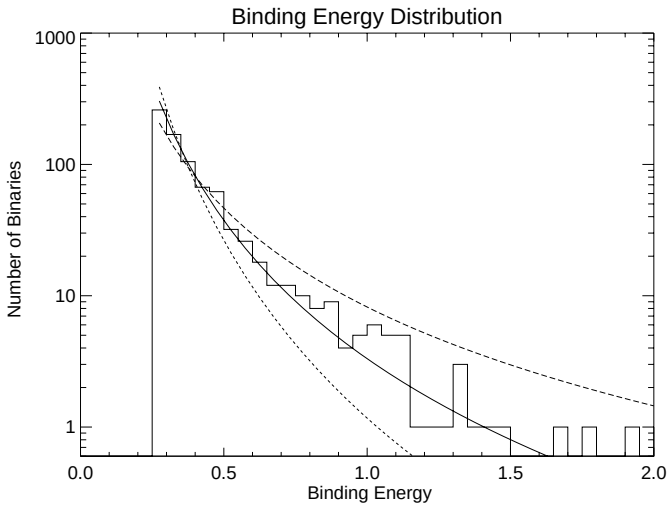

Fig. 2. Binary binding energy distribution for $N = 3$ equal masses. The dashed, solid, and dotted curves are analytic fits with $\gamma = 5/2$, 7/2, and 9/2, respectively.

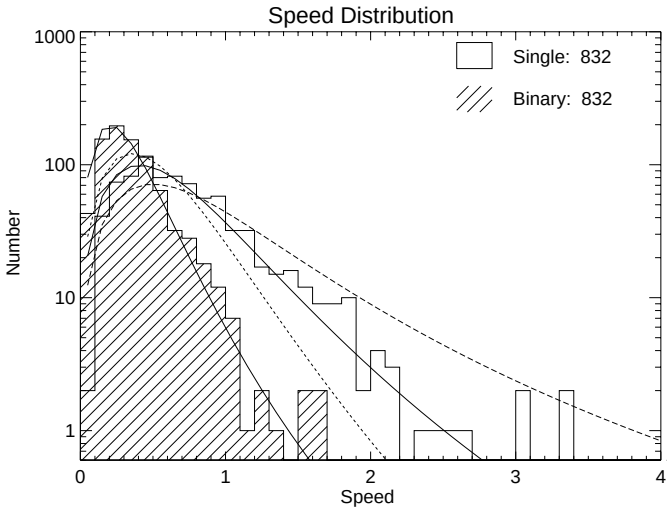

Fig. 3. Speed distribution of single and binary remnants for N = 3 equal masses. Curve types have the same meanings as in Fig. 2.

This choice is reinforced by comparing the computed speed distributions for remnant singles and binaries with Eqs. (12) and (13), as illustrated in Fig. 3. To avoid clutter, only the $\gamma = 7/2$ curve is plotted for the binaries. For equal masses, the mapping from E_b to a is one-to-one. So, the same 7/2 choice of γ must be used to fit g_a for self-consistency, and in fact it is also very good (see Fig. 5 below). The general properties of the g_E and g_s in our experiments have been noted in earlier three-body research, going back to Saslaw et al. (1974); but our determination of the γ governing the underlying physics seems better, perhaps because we follow the decay process longer and do not use approximate escape criteria.

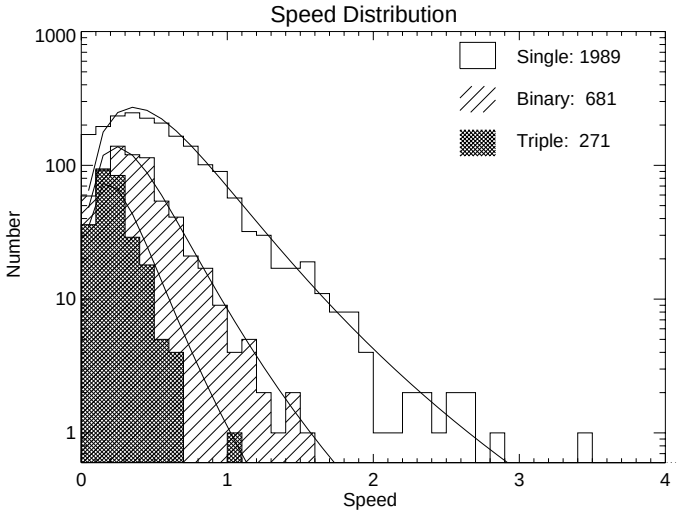

Fig. 4. Speed distribution for single, binary and triple remnants for N = 5 equal masses. Only analytic fits for $\gamma = 7/2$ are shown.

3.3.2. $N = 4$ and 5

As N increases, it is not clear *a priori* that Eq. (8) should work as well. Table 1 does indicate the predominance of one hard-binary formation event in disrupting the systems. We have examined figures like Fig. 2 where we include only the BS channel binaries, all binaries (BS, BBS, and TB), and all binaries plus the inner binaries of triples. Some of the BBS and TB binaries are only weakly bound and do not at all fit a power law, but their numbers are small. Ragardless of how we construct the g_E diagram, we again judge that $\gamma = 7/2$ gives the best fit to the hard-binary distribution for both $N = 4$ and 5. Even more surprising is that Eq. (15) gives a remarkably good fit to the velocity data for singles, binaries, and triples, as illustrated in Fig. 4 for $N = 5$. One exception is a noticable excess of relatively slow escaping singles which also occurs to a lesser degree for $N = 4$. The goodness of the analytic fit does have a physical implication. The underlying assumption that the single escapers share equally in the escape energy must be roughly true overall. One might have expected instead to have a far greater excess of slow escapers and only one star per system carrying away most of the energy.

The binary separation distribution for all binary remnants, along with the $\gamma = 7/2$ version of Eq. (9), is shown in Fig. 5 for $N = 3$, 4, and 5. Binary subcomponents of triples and quadruples are not included. As N increases, smaller binary separations are achieved primarily because m is smaller. There is more smearing away from the power law as N increases in part because one of the binaries from the BBS channel and binaries from the TB channel are usually only loosely bound.

Remarkably, after studying plots like Fig. 2

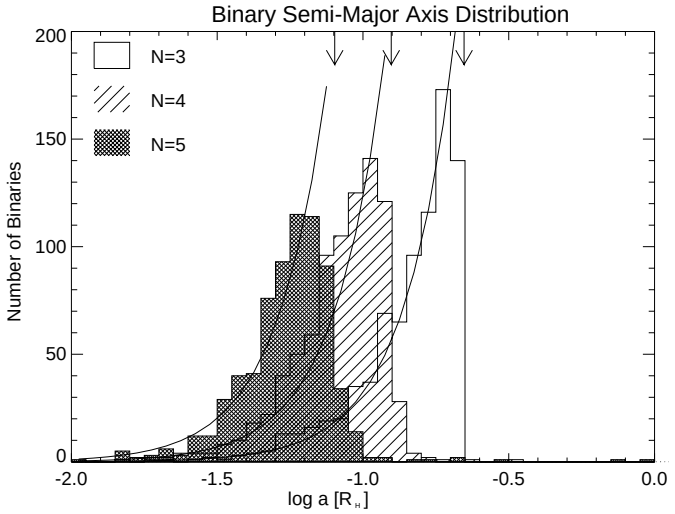

Fig. 5. Binary semi-major axis distributions for N = 3, 4 and 5 equal masses together with $\gamma = 7/2$ analytic fits. The arrows along the top indicate the locations of $a = a_{max}$ for N = 3, 4, and 5 from right to left.

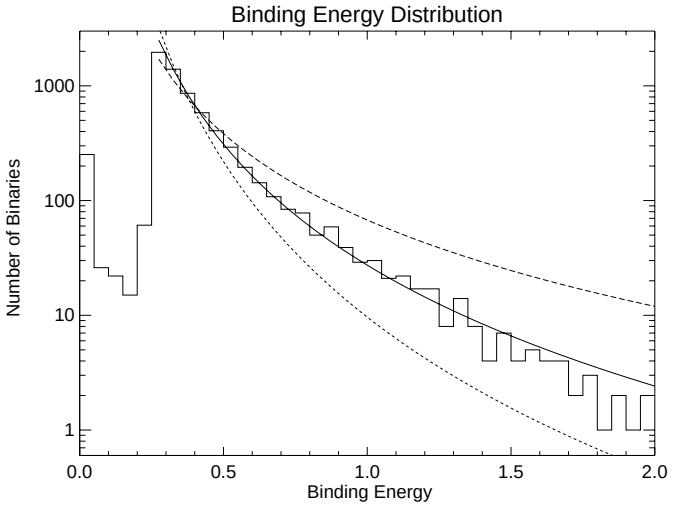

Fig. 6. The distribution of binary binding energies for all N and f combined. Curve types have the same meanings as in Fig. 2.

3.4. Realistic mass spectra

3.4.1. The $\gamma = 7/2$ $|E_b|$-distribution

for unequal masses, we conclude that, for the low angular momentum ($\alpha = \beta = 0$) spherical cases considered in this paper, the binary energy distributions all obey essentially the same $\gamma = 7/2$ power law regardless of N or f. To illustrate this point with the best possible statistics, Fig. 6 combines the data for the 6,863 binary remnants from all nine experiments listed in Table 1. Except for the loosely bound binaries contributed by the BBS and TB channels, the $\gamma = 7/2$ law evidently is an excellent fit. Preliminary experiments for high angular momentum systems and for systems with extreme geometries, which are the subject of the next paper in this series, do show different power laws; and we defer until then a discussion of what factors determine the appropriate γ.

Table 8. Escape speed distributions for single stars.

N	f	v	data	7/2	5/2	9/2
	EM	50%	.62	.57	.77	.47
		90%	1.33	1.23	1.91	.96
3	CM	50%	1.11	1.12	1.52	.93
		90%	2.75	2.44	3.79	1.92
	MS	50%	1.21	1.24	1.68	1.02
		90%	3.08	2.69	4.18	2.11
	EM	50%	.52	.49	.67	.41
		90%	1.13	1.07	1.66	.84
4	CM	50%	.85	.87	1.18	.72
		90%	2.01	1.89	2.93	1.48
	MS	50%	.93	.98	1.34	.82
		90%	2.18	2.14	3.32	1.68
	EM	50%	.47	.49	.67	.41
		90%	1.03	1.07	1.66	.84
5	CM	50%	.74	.77	1.04	.63
		90%	1.76	1.67	2.59	1.31
	MS	50%	.87	.88	1.20	.78
		90%	2.16	1.92	2.99	1.51

3.4.2. Escape speeds

Table 8 summaries two important features of the escape speed distributions for single stars. Typical speeds are indicated by quoting the median speed (labelled 50%), and the nonGaussian high-velocity tail of the speed distribution is characterized by giving the speed for which 90% of the stars move more slowly in the cumulative distribution. Shown, for comparison are the same quantities obtained from the analytic distributions (12), (14), and (17) for the best-fit $\gamma = 7/2$. As a quantitive measure of the superiority of this fit, the same velocities are also tabulated for $\gamma = 5/2$ and 9/2. The agreement between the data and $\gamma = 7/2$ is usually within about 10% and tends to get better as N increases. With only a few exceptions, the speeds for 5/2 or 9/2 tend to be off by more like 20–50%.

Table 8, of course, manifests the same physical trends as Table 3. Escape speeds increase as f^* becomes broader, due to the lower masses of the escapers, and decreases with increasing N because there are more objects sharing the energy released by hard-binary formation. About half the single escapers end up with speeds $\sim v_{vir} \approx 0.71$, but the distribution is significantly nonGaussian. Fully 10% of the stars have speeds which are greater than the median by factors of 2.2 for equal mass cases and of 2.3–2.5 for unequal masses. The precise ratio expected for the analytic $\gamma = 7/2$ fit is 2.18. About one percent of the escapers have speeds over four times the median speed. Figs. 7a and 7c show the full escape speed distributions for all single, binary, and triple remnants drawn from f_{cm}.

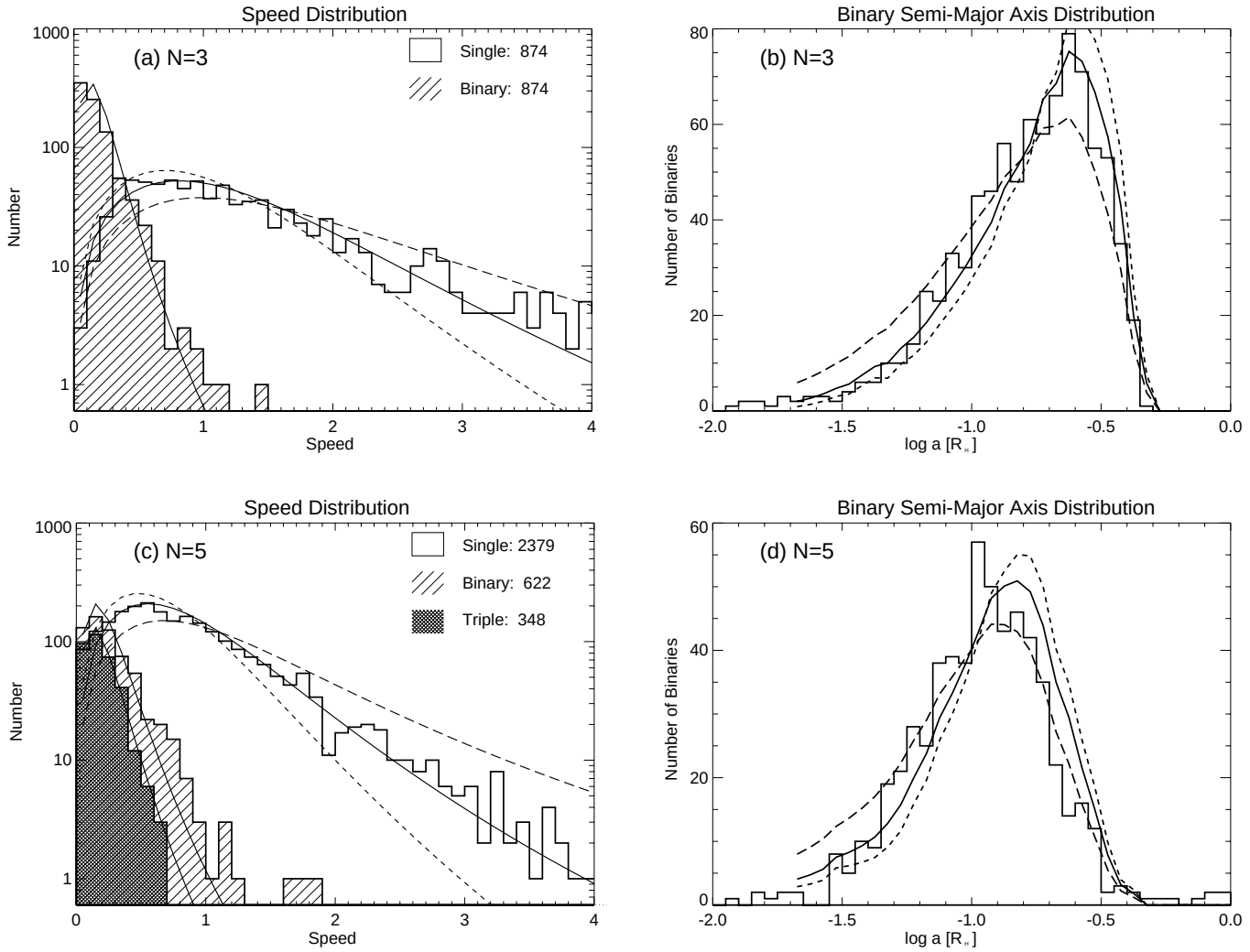

Fig. 7a–d. Results for the clump mass spectrum CM: remnant speed (**a**) and binary semi-major axis (**b**) distributions for $N = 3$; (**c**) and (**d**), the same for $N = 5$. Curve types have the same meanings as in Fig. 2.

3.4.3. Binary and multiple characteristics

Figs. 7b and 7d illustrate the binary semi-major axis distributions for $N = 3$ and 5 with the CM spectrum and can be compared with Fig. 5 for the case of equal masses. In Fig. 7b, the best fit is obtained with the semi-analytic $\gamma = 7/2$ "shark-fin" function, where the numerically determined $g_{ij}(m_i m_j)$ is used in Eq. (20). The fit is not as good for $N = 5$. The apparent shift of the experimental results to about 20% smaller values of a is due in part to the fact that, even for equal masses, the $N = 5$ peak is not as sharp and is shifted to the left of $a = a_{max}$. The agreement is better for CM with $N = 4$ and for all the MS cases.

Table 9 gives the peaks and FWHM of the analytic functional fits to the semi-major axis distributions. In all cases, these are within 10–20% of the values which would be judged by eye from the histograms. Note that, as in the diagrams, the distributions are here considered to be per unit $d\log_{10}a$ not per unit da interval. For the realistic unequal mass case, the sharp power law becomes smeared out largely because of the range of possible binary mass products $m_i m_j$. For all unequal mass cases, the peak of the semi-major axis distribution is $\log_{10}a \approx -0.72 \pm 0.1$ and the FWHM $\Delta\log_{10}a \approx 0.55 \pm 0.1$ with a tendency for the peak to shift to smaller a as N increases. In other words, the binaries formed by the decay of $N = 3$ to 5 systems tend to have semi-major axes about five times smaller than the origi-

Table 9. Peak and full-width-at-half-maximum of the binary separation distributions.

N	f	$\log_{10}a$	$\Delta\log_{10}a$
3	EM	-0.65	0.12
	CM	-0.63	0.53
	MS	-0.63	0.60
4	EM	-0.90	0.12
	CM	-0.72	0.47
	MS	-0.65	0.65
5	EM	-1.10	0.12
	CM	-0.82	0.57
	MS	-0.72	0.58

nal few-body system size R_H, distributed with a FWHM that covers a range of about a factor 3 or 4 in a.

4. Applications

In Sect. 3, we used only dimensionless variables. Here, we first consider several aspects of the results in physical units which depend only on the physical stellar masses, namely the multiplicity fractions as a function of mass bin and the mass ratios of the remnant binaries. Then, we apply an additional physical scaling to derive speed and binary separation distributions in physical units. Although we make some comparisons with observations, the analyses in this section are only illustrative of the possible effects of few-body decay on star formation. Definitive results require input not yet available concerning initial cloud core conditions and reliable statistical mappings from these conditions to few-body outcomes of cloud collapse and fragmentation.

4.1. Multiplicity fractions

Going back to the original physical masses, we divide the stars into four mass bins which give roughly equal numbers of stars for the CM spectrum. The labels are meant to reflect the approximate spectral types that stars of these masses would have on the main sequence:

M: Late M-type stars, $0.1M_\odot \leq M \leq 0.2M_\odot$
MK: M & K-type stars, $0.2M_\odot < M \leq 0.5M_\odot$
KG: Solar-type stars, $0.5M_\odot < M \leq 1.2M_\odot$
F+: F-type stars & earlier, $1.2M_\odot < M \leq 10M_\odot$

We do not bin more finely in order to have good statistics. Table 10 summaries the multiplicity fractions within each group. The "total" here refers to the total number of remnant systems whose most-massive star (primary) is in the mass bin, and we emphasize that the multiplicity fractions are only for systems with primaries in the mass bin by adding a subscript p.

The results for the MS mass spectrum exhibit features described by McDonald & Clarke (1993, see also van Albada 1968a, Valtonen 1997, 1998). Because of dynamical biasing, when simply selecting stars from a realistic IMF for small N without dissipation, it is very difficult to achieve a reasonable distribution of BF_p's along the main sequence. Also, the lowest-mass stars (or brown dwarfs) allowed by the fragmentation IMF tend to be entirely single and to dominate the population of remnants escaping with moderate to high speeds. In real SFR's, however, one expects there to be a spectrum of cloud masses undergoing collapse. Then the total few-body system mass that results is constrained by the clump mass, and lower-mass stars can sometimes end up as the most-massive and hence binary-producing stars in their system. The CM systems are in fact constructed in this way and, as a result, exhibit a more realisitically uniform distribution of SF's and BF_p's among the mass bins. It is still the case that the lowest-mass objects are almost entirely singles, but now there are also nonnegligible BF_p's even for the MK bin. There is a distinct tendency for both f's to produce rather large fractions of higher multiplicity systems for F+ with $N = 4$ and 5.

Table 10. Multiplicity fractions for remnant systems with primaries in four mass bins.

N	f	mass	total	SF	BF_p	TF_p	QF_p
	CM	M	437	1.00	.00	.00	
		MK	399	.82	.15	.03	
		KG	472	.19	.72	.09	
3		F+	558	.03	.86	.11	
	MS	M	388	.98	.01	.01	
		MK	338	.81	.15	.04	
		KG	301	.47	.46	.07	
		F+	832	.10	.82	.08	
	CM	M	832	1.00	.00	.00	.00
		MK	794	.81	.15	.04	.00
		KG	545	.32	.52	.13	.03
4		F+	505	.07	.73	.16	.04
	MS	M	552	1.00	.00	.00	.00
		MK	601	.95	.03	.02	.00
		KG	434	.80	.15	.04	.01
		F+	1098	.22	.64	.12	.02
	CM	M	1270	.99	.01	.00	.00
		MK	1133	.75	.15	.10	.00
		KG	568	.40	.35	.19	.06
5		F+	440	.09	.56	.29	.06
	MS	M	695	1.00	.00	.00	.00
		MK	776	.97	.02	.01	.00
		KG	630	.89	.07	.03	.00
		F+	1338	.32	.44	.21	.02

An increasing binary fraction with primary mass is an established observational fact, at least for main-sequence stars. For M-dwarf primaries the reported binary frequencies are in the range of $26 \pm 9\%$ (Leinert et al. 1997) to $42 \pm 9\%$ (FM). FM find a ratio of about 4:1 for the appearance of binary to higher-order systems. The G-dwarf binary frequency is higher, estimated to be $57 \pm 9\%$ (DM). For masses in the F+ range, observations suggest even higher binary frequencies, but at lower statistical significance (see, e.g., Abt et al. 1991, McAlister et al. 1993, Petr et al. 1998).

We do not expect that the statistical outcome of our simulations will match the observed quantities in every respect. We know, for instance, that our initial conditions in this paper (zero angular momentum, spherical, no remnant gas) are probably not realistic outcomes of fragmentation. It is also likely that cloud fragmentation will lead to a distribution of N's. However, the general trends of the BF_p distributions in our CM simulations are in agreement with observed trends. Because $N = 4$ with a CM spectrum comes closest to observed multiplicity values, we concentrate the subsequent analysis on this case.

4.2. Mass ratios

Observations also suggest trends in the distribution of binary mass ratio $q = M_2/M_1$ as a function of primary mass. For G-dwarf primaries (DM), the number of secondaries increases as q

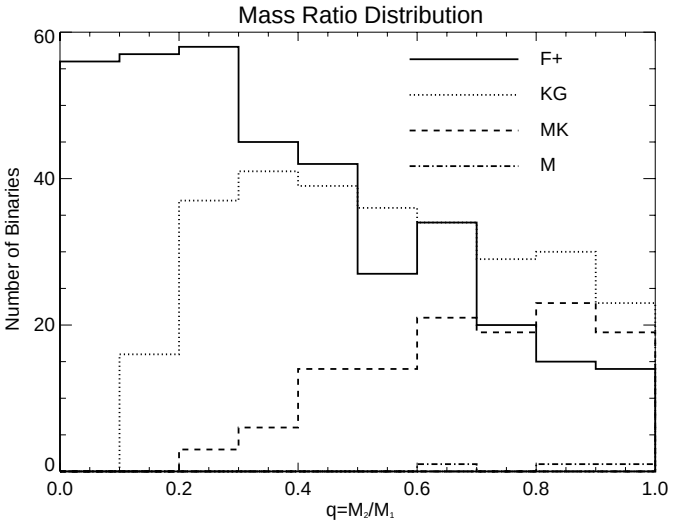

Fig. 8. The distribution of binary mass ratios for N = 4 and the CM spectrum. Curve types refer to the primary mass bins defined in the text.

decreases and peaks near $q = 0.2$–0.4. Very low-mass companions ($q = 0.0$–0.1) seem to be rare. On the other hand, FM show that the q-distribution for M-dwarf primaries is relatively flat and possibly even decreases as q decreases; but their results are restricted to the range $q = 0.4$–1.0 to avoid a selection-loss bias for the lowest-mass secondaries. Fig. 8 shows the q-distributions from the N = 4 CM spectrum for our four primary mass bins. Our MK and KG mass bins exhibit q-distributions with characteristics similar to those reported by FM and DM, respectively.

This match of the mass-ratio distributions is a natural consequence of binary formation in decaying, small-N clusters. In 1968, van Albada already described the general tendencies. Using a modern IMF and assuming pure dynamical biasing of the formed binary, McDonald & Clarke (1993, 1995) found they were able to fit the observed distributions of BF_p and q, provided they included effects of dissipative encounters. More recently, Valtonen (1997, 1998) found reasonable agreement in the q-distributions of wide binaries by applying Monaghan's (1976a, 1977) statistical theory for three-body encounters. In particular, he showed that the Tokovinin (1997) multiple-star catelog exhibits trends with primary mass similar to those in our Fig. 8. Our work strengthens these results, because we are deriving the binary properties directly with a high-precision numerical integrator. We match the observed trends in BF_p and q without appeal to the dissipative effects of gas by using the two-level IMF of the CM spectrum.

4.3. Speed and binary semi-major axis distributions

Results presented so far are applicable to any gravitationally bound, point-mass system evolving under mutual gravitational forces. Two characteristic scales are necessary to determine a complete set of physical units in this case. These can be a characterisitc length and time, or an energy and a mass, or any other two independent quantities in Eqs. (1) to (3). As discussed in the preceeding section, binary fractions and mass ratio distributions are fully described by scaling M_{tot} back to its dimensional value. Speed and binary semi-major axis distributions can then be given in dimensional units only when an additional scaling is applied, but there are many ways to do this.

It is at this level where we are forced to introduce further assumptions about the conditions that are realistic and typical for early stages of low-mass star formation. In SD, we gave arguments for the choice of typical total system masses and sizes based on outcomes of fragmentation calculations. A total system mass $M_{tot} = 3M_\odot$ appears to be consistent with the stellar mass fraction within typical fragmenting cloud cores. Typical separations of the "seeds" in fragmentation calculations are ~ 100 A.U.; SD used $R_H = 125$ A.U. These choices of R_H and M_{tot} imply $v_{vir} = (GM_{tot}/2R_H)^{1/2} = 3.3$ km/s.

In a given SFR, it is plausible that the M_{tot} and R_H resulting from fragmenting collapses are related due to correlations in pre-collapse cloud properties. It is also possible that there might be some dispersion in these parameters, as well as a variety of N-values. It is beyond the scope of this paper to define such relations or distributions. Instead, for illustrative purposes, we assume there is a relation of the form $R_H \propto M_{tot}^{\zeta}$ and consider three limiting cases which allow easy scaling and a direct application of results from Sect. 3:

1. $\zeta = 0 \Rightarrow R_H =$ constant. We choose the SD value $R_H =$ 125 A.U. For this case, $E_0/M_{tot}^2 =$ constant and $v_{vir} \propto M_{tot}^{1/2}$.
2. $\zeta = 1 \Rightarrow v_{vir} =$ constant. Again, we use the SD value of 3.3 km/s. This scaling law results in a constant specific energy for each few-body system, i.e., $E_0/M_{tot} =$ constant. A relation of this type could result if fragmentation during isothermal collapse occurred below some threshold ratio of thermal to gravitational energy.
3. $\zeta = 2 \Rightarrow E_0 =$ constant. Using the SD choices, $|E_0| = 3.2 \cdot 10^{44}$ ergs. For this case, $v_{vir} \propto M_{tot}^{-1/2}$.

In Figs. 9a and b, we compare the speed and the binary semi-major axis distributions in physical units for these three scaling relations using $N = 4$ and the CM spectrum. The full lines correspond to the $\zeta = 1$ scaling law. Fig. 9a displays the speed distribution for single stars. According to the nondimensionalization resulting from (1) and (2), the velocity unit in Sect. 3 corresponds to $(GM_{tot}/R_H)^{1/2} = \sqrt{2}v_{vir}$. So, the $\zeta = 1$ curve in Fig. 9a results simply from multiplying the dimensionless speeds (as in Figs. 7a and 7c) by the constant $\sqrt{2}v_{vir} = 4.6$ km/s. This distribution is bracketed by the $\zeta = 0$ (dotted) and $\zeta = 2$ (dashed) cases, which give broader and narrower distributions, respectively. In Fig. 9b, it is the $\zeta = 0$ case for which the dimensionless a's need only be multiplied by the constant scale factor R_H. The $\zeta = 1$ and $\zeta = 2$ cases are broadened by the M_{tot}-dependence of the R_H scale factor. Figs. 9c and d show the speed and semi-major axis distributions with $\zeta = 1$ for each of the mass bins defined in Sect. 4.1.

In Table 11, we compile results for the following observable quantities by mass bin for the particular case $\zeta = 1$: a) one-dimensional velocity dispersions for single stars (in km/s), b)

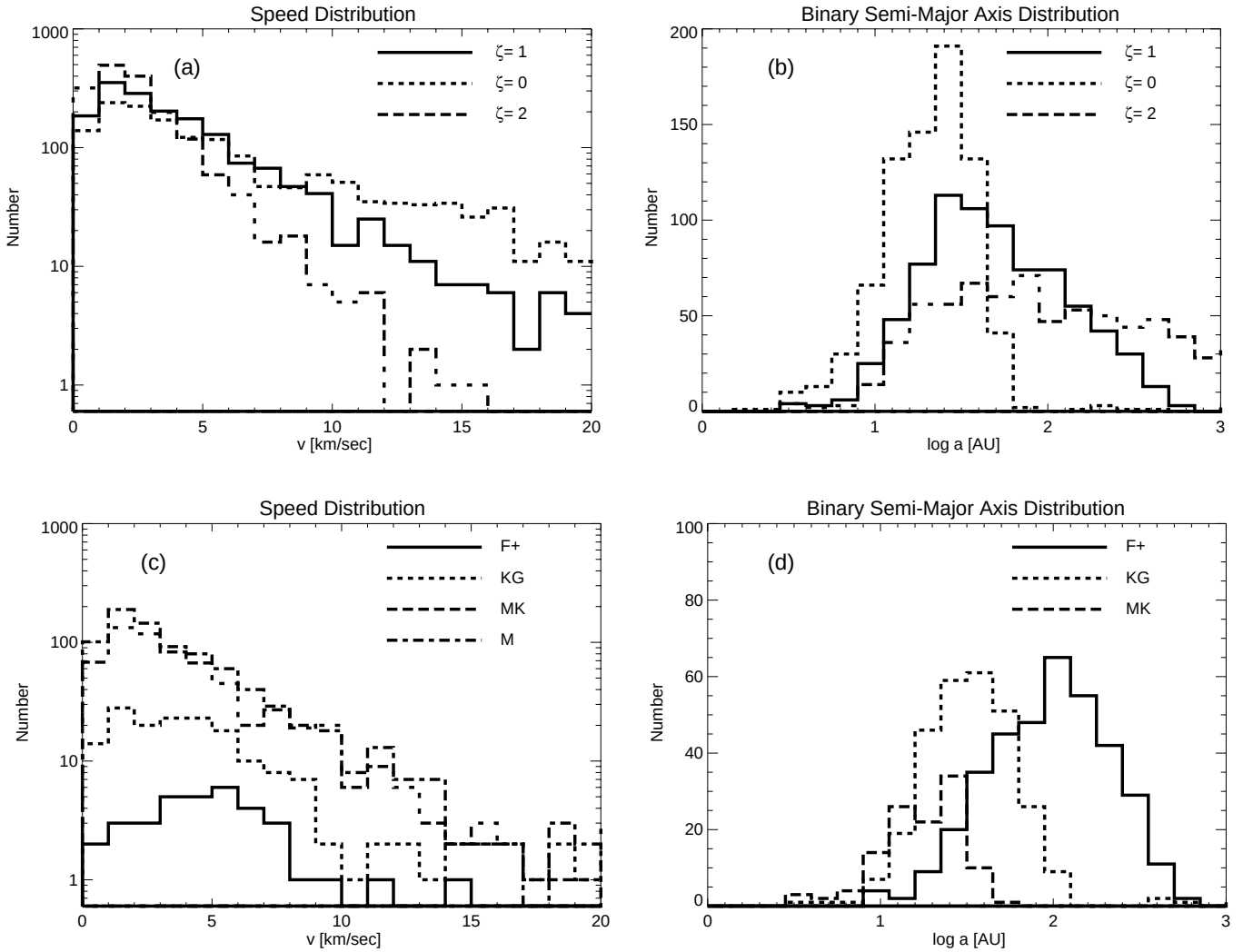

Fig. 9a–d. Scaled results for the CM spectrum and N = 4: **a** single remnant speeds for ζ = 0, 1 and 2 in km/sec **b** binary semi-major axis distributions for ζ = 0, 1 and 2 in A.U. **c** remnant speeds for ζ = 1, curve types refer to mass bins **d** binary semi-major axis distributions for ζ = 1, curve types refer to mass bins.

one-dimensional velocity dispersions for primaries in binaries (in km/s), c) the mean binary semi-major axis (in A.U.), d) the standard deviation of the binary semi-major axis distribution expressed as a distribution in $\log_{10} a$ (in dec's). A number of important conclusions can be drawn from Table 11:

1. For $N > 3$, typical one-dimensional velocity dispersions for single stars are in the range 3–4 km/s, largely independent of $f(M)$, N, and the mass bin.
2. For $N = 3$, the velocity dispersions vary with stellar mass from 2–3 km/s (for F-type stars) up to 5–6 km/s (for M-type stars).
3. The COM velocity dispersions for binaries are lower than those of single stars but are not negligible. They are typically a factor 3 to 6 times smaller than those for the single stars.
4. The typical mean semi-major axis is $\sim$ 30 A.U. with a shift toward larger separations ($\sim$ 100 A.U.) for the earlier-type stars and toward smaller separations ($\sim$ 10 A.U.) for the latest types.
5. The standard deviation of the semi-major axis distribution in a mass bin is typically a factor of 2.

It is important to remember that, although we quote velocity dispersions here, the velocity distribution is distinctly nonGaussian and has a power-law high-velocity tail. Conclusions 1, 2, and 4 above are sensitive to the choice of ζ; conclusions 3 and 5 are not.

4.4. Implications for star formation

If multiple fragmentation during cloud collapse, followed by dynamic decay of the few-body system, is a frequent mode of star formation, then specific signatures will be imprinted on the endproducts. This imprinting should mostly occur soon after fragmentation, typically within tens of T_{cr} or $\sim 10^4$ yrs, and will be preserved over a much longer time, provided that no further dynamic interactions with other components of the SFR takes place. In this sense, our results should be more relevant

Table 11. One-dimensional velocity dispersions for single stars and binaries in km/s, plus means in A.U. and standard deviations in dec's of the binary semi-major axis distributions for $\zeta = 1$ and $v_{vir} = 3.3$ km/s. Stars indicate poor binary statistics for that mass bin; no entry means a complete absence of binaries.

N	f	mass	σ(S)	$\sigma(B_p)$	$\bar{a}$	$\sigma(a)$
	CM	M	5.5			
		MK	4.6	0.8	23	0.20
		KG	4.0	0.7	30	0.26
3		F+	2.2	0.5	69	0.36
	MS	M*	6.9	1.4	7	0.25
		MK	6.3	1.0	14	0.24
		KG	4.4	0.9	32	0.30
		F+	3.6	0.5	123	0.44
	CM	M	3.5			
		MK	3.4	1.1	17	0.44
		KG	3.4	0.8	28	0.29
4		F+	4.3	0.6	78	0.35
	MS	M	4.3			
		MK*	3.9	1.7	30	0.92
		KG	3.6	0.9	35	0.30
		F+	3.3	0.6	145	0.41
	CM	M*	3.0	1.6	204	1.28
		MK	3.0	1.2	17	0.59
		KG	3.1	0.9	28	0.37
5		F+	3.0	0.7	76	0.32
	MS	M	3.8			
		MK*	3.7	1.2	63	1.10
		KG	3.5	1.1	63	0.88
		F+	3.4	0.8	170	0.45

to loose T Associations like Taurus than to densely clustered SFR's like Orion. However, molecular clouds exhibit a broad spectrum of length scales and core masses. The few-body systems considered here might be subcomponents of larger clusters or groups, like those considered by Kroupa (1995, 1998), and could have a significant influence on their dynamical evolution.

Independent of any scaling assumptions, we have shown that the typical binary semi-major axis for remnants of few-body decay is ~ 5 times smaller than the original few-body system size. This step bridges the length scale from typical cloud collapse outcomes (100's A.U.) to typical binary separations (10's A.U.), a reduction in scale which is otherwise not well understood.

Our application of physical scalings which are consistent with available observational and theoretical constraints yields interesting results for remnant velocities, binary frequencies, and binary mass ratios. For the $\zeta = 1$ example given in the preceeding section, the difference in dispersion velocities for single stars (3–4 km/s) and binaries ($\leq$ 1 km/s) would cause spatial segregation of these remnants over time. A careful analysis of the BF in a SFR should therefore take into account the possibility that single stars may be dispersed over a few times larger radial extent around the birth site than multiple stars of the same age. Single TTS as old 10^7 yrs could fill a sphere with a radius ~ 50 pc, a volume not easily surveyed by conventional observational methods for discovering young stars. If $\zeta \approx 1$, even single G, F, and A-type stars can obtain roughly the same large dispersion speeds as those of single M and K-type stars, a result which surprised even us. The recent ROSAT-discoveries of broad spatial distributions of young stars (see Sect. 1.3) could, in part, be a manifestation of large dispersion velocities caused by few-body decays. Although we have not included substellar mass objects in our IMF, it is clear from our results for the M mass bin that these would all be ejected as single bodies. A spectacular HST/NICMOS observation shows a very cool object near a young binary in Taurus. This could be an escaping planet or brown dwarf which has been dynamically ejected in the manner considered here (Terebey et al. 1998).

By adopting the reasonable assumption that there is a cloud mass spectrum which constrains the choice of fragment masses, leading to the two-step IMF of the CM spectrum, we have shown that observed trends in binary fractions and mass ratio distributions can be matched even by simple gas-free few-body decays. This strengthens the classic notion (see Sects. 1.1 and 1.3) that N-body decay has played a significant or dominant role in shaping these properties of binary stars.

4.5. Strengths and limitations

We have characterized the statistical outcome of few-body decay, with emphasis on multiplicity fractions, speed distributions, and binary properties. Here, the decay is viewed as one step in the overall process of star formation. We cannot present definitive results because critical input is lacking, namely, the distribution of cloud collapse outcomes, the N's, M_{tot}'s, R_H's, $f(M)$, etc. In this paper, we have considered only rather unrealistic zero angular momentum systems; but we plan to include effects of extreme fragment geometries and initial velocity fields in our next paper. A more fundamental limitiation is that we omit all effects of continued gas accretion by the few-body system (McDonald & Clarke 1995, Bonnell et al. 1997), a difficiency that will be difficult to remedy with our current orbit integrator. We also ignore the possibility of star/star collisions or tidal interactions and have not attempted to keep track of closest approaches. For most of our resulting binaries, with separations of 10's A.U., this is probably not a concern, because low-mass stars typically have radii only a few times larger than the Sun's. Of course, if the stars have disks, star/disk and disk/disk collisions will be important (McDonald & Clarke 1995). For these reasons, our pure point-mass treatment is not directly applicable to the origin of close binaries ($<$ A.U.).

Despite these limitations, we have, in some respects, been more successful than expected. For the zero angular momentum case, we now have precise results which can be readily adopted by other researchers, like McDonald & Clarke (1993) or Valtonen (1997, 1998), who study implications of few-body decay without recourse to orbit integration. Statistical selections of mass configurations can now be mapped to multiplicity fractions which include first-order corrections to pure-BS and pure dynamical biasing assumptions. We have also derived and tested precise analytic approximations for the speed distribu-

tions of all remnants and for the semi-major axis distribution of binaries. Many aspects of these results have proven to be fairly insensitive to the precise choice of $f(M)$, except that the BF$_p$'s and q-distributions show more realistic trends with mass when a two-step IMF is used. As realistic conditions and outcomes of cloud collapse become better defined, our mappings to final stellar remnant distributions, as well as the tools to produce additional such mappings, will be available.

5. Conclusions

We have performed a statistical study of complete few-body decay for N = 3, 4, and 5 using direct orbit integrations and a novel analysis technique. For N = 4 and 5, these are the first such results available from a modern few-body code that we are aware of. Our main conclusions divide naturally into contributions to few-body stellar dynamics theory and applications to star formation.

Stellar Dynamics. The combination of long integrations and our hierarchical virtual-particle analysis has permitted us to characterize the complete decay, i.e., to identify the independent, long-lived, bound remnants and their kinematics. These results completely supercede those of Harrington (1974, 1975) for $N = 4$ and 5. Viewing the decay as a general physical process and studying a 1,000 system realizations, we have obtained precise values (within $\pm$ 0.02 or less) for the "branching ratios" between possible decay channels. Many overall results are in accord with classic expections, although there are significant refinements. Decays are dominated by the production of a single hard binary, but the binary plus $N - 2$ singles decay channel is not the only important mode of decay, especially as N increases. Branching ratios are sensitive to N and somewhat more weakly to the mass spectrum $f(M)$. On the other hand, the multiplicity fractions are sensitive to N, but not to $f(M)$. Dynamical biasing is only violated at the 10–20% level.

For the zero angular momentum initial system conditions considered in this paper, we find that the distribution of binding energies for the hard remnant binaries is extremely well-matched by an $|E_b|^{-\gamma}$ Heggie Law with $\gamma = 7/2$. This is distinctly different from the 9/2 suggested by Heggie himself (1975) for bound three-body systems and the 5/2 advocated by Monaghan (1976a). The law is sufficiently precise and the hard binary sufficiently dominates the energetics of decay that analytic expressions for the escape speeds of single and multiple remnants can be derived which accurately reproduce the computational results for all N and f. The same is true for the distribution of binary semi-major axes. In general, for unequal mass systems, the binaries formed have semi-major axes ~ 5 times smaller than the original virial system size with a full width at half maximum of about a factor of 3 to 4.

Star Formation. If cloud collapse and multiple fragmentation, followed by dynamic decay of the fragment system, is a common mode of star formation, then our results imply several observational consequences. A two-step IMF, like our clump mass spectrum, where fragment mass choices are constrained by the mass distribution of collapsing clouds, shows considerable promise for reproducing observed trends in binary fractions and binary mass ratio distributions along the main sequence, even for gas-free decay. Although the lowest-mass objects in the overall IMF always end up being ejected as singles, even stars only a few times more massive than the lower cut-off can have a significant binary fraction. At the same time, quite massive stars can have a nonnegligible fraction of singles.

The generic reduction of a factor of five in the semi-major axes of our binaries compared with the initial system size may help explain why binary separation distribution for solar-type stars peaks at $\sim$ 10's A.U. (DM), while collapse calculations for reasonable initial cloud parameters give typical fragment system sizes $\sim$ 100's A.U. It is difficult to be as definitive about the kinematic consequences of few-body decay during star formation, because more needs to known about the initial few-body system properties. However, some plausible examples discussed in this paper show that significant escape speeds (one-dimensional velocity dispersions $\sim$ 3–4 km/s) can be attained by single stars of all masses and that the lower speeds of the binaries and multiples ($\leq$ 1 km/s) would result in spatial segregation of remnant types over time. The latter sounds a cautionary note regarding the completeness of SFR binary frequency surveys. The speed distributions are distinctly nonGaussian and have a power-law high-speed tail.

Future papers in this series will consider initial few-body conditions with nonzero velocities and nonspherical geometries and will include at least some effects of background and/or accreting gas. We also plan to make simple kinematic models of SFR's hypothetically dominated by this mode of star formation.

Acknowledgements. We thank S. Aarseth, who kindly provided to us the latest version of the integration program CHAIN. Thanks also to A. Burkert, C. Clarke, T. Hartquist, L. Kiseleva, P. Kroupa, E. Levy, C. McKee, B.K. Pickett, and H. Zinnecker for useful conversations and encouragement. This work was supported in part by the DFG, by NASA Grants NAGW 3399 and NAGW5-4342, and by the Alexander von Humboldt Foundation.

References

Aarseth S. J., Anosova J. P., Orlov V. V., Szebehely, V. G., 1994a, Cel. Mech. Dyn. Astr. 58, 1

Aarseth S. J., Anosova J. P., Orlov V. V., Szebehely V. G., 1994b, Cel. Mech. Dyn. Astr. 60, 131

Abt H.A., Wang R., Cardona O., 1991, ApJ 367, 155

Alcalá, J.M., Krautter, J., Schmitt, J.H.M.M., Covino, E., Wichmann, R., Mundt, R., 1995, A&AS, 114, 109

Alcalá, J.M., Krautter, J., Covino, E. et al., 1997, A&A 319, 184

Anosova J.P., 1969, Astrophysics 5, 81

Anosova J.P., Kirsanov N.O., 1991, Comments Ap 15, 283

Anosova J. P., Orlov V. V. (AO), 1994, Cel. Mech. Dyn. Astr. 59, 327

Anasova J. P., Orlov V. V., Aarseth S. J. (AOA), 1994, Cel. Mech. Dyn. Astr. 60, 365

Bate M. R., Burkert A., 1997, MNRAS 288, 1060

Black D.C., 1982, AJ 87, 1333

Bodenheimer P., Ruzmajkina T., Mathieu R. D., 1993, Stellar multiple systems - Constraints on the mechanism of origin. In: Protostars and Planets III, 367

Bodenheimer P., 1995, ARAA 33, 199
Bonnell I., Arcoragi J.-P., Martel H., Bastien P., 1992, ApJ 400, 579
Bonnell I. A., Bate M. R., Clarke C. J., Pringle J. E., 1997, MNRAS 285, 201
Boss A.P., 1988, Comments Ap 12, 169
Boss A.P., 1993, ApJ 410, 157
Boss A. P., 1996, ApJ 468, 231
Bouvier J., Rigaut F., Nadeau D., 1997, A&A 323, 139
Brandner W., Köhler R., 1998, ApJL 499, L79
Burkert A. Bodenheimer P., 1993, MNRAS 264, 798
Burkert A., Bodenheimer P., 1996, MNRAS 280, 1190
Burkert A., Bate M. R., Bodenheimer P., 1997, MNRAS 289, 497
Burkert A., Klessen R., Bodenheimer P., 1998, In: The Orion Complex Revisited. Eds. A. Burkert & M. McCaughrean (ASP: San Francisco), in press
Clarke C.J., Pringle J.E., 1991, MNRAS 249, 588
Clarke C.J., Pringle J.E., 1993, MNRAS 261, 190
Covino E., Alcala J.M., Allain S. et al., 1997, A&A 328, 187
Duquennoy A., Mayor M. (DM), 1991, A&A 248, 485
Durisen R.H., Sterzik M.F., 1994, A&A 286, 84
Eggelton P., Kiseleva L. (EK), 1995, ApJ 455, 640
Elmergreen B.G., Falgarone E. 1996, ApJ 471, 816
Fischer D.A., Marcy G.W. (FM), 1992, ApJ 396, 178
Ghez A., Neugebauer G., Matthews K., 1993, AJ, 106, 2005
Guillout P., Sterzik M.F., Schmitt J.H.M.M et al., 1998, A&A 334, 540
Harrington R.S., 1974, Celest.Mech. 9, 465
Harrington R.S., 1975, AJ 80, 1081
Hartmann L., Stauffer J.R., Kenyon S.J., Jones B.F., 1991, AJ 101, 1050
Heggie D.C., 1975, MNRAS 173, 729
Heggie D.C., Mathieu R.D., 1986, In: The Use of Supercomputers in Stellar Dynamics. Eds. P. Hut & S.L.W. McMillan (Springer-Verlag: New York), p. 233.
Heggie D.C., Sweatman W.L., 1991, MNRAS 250, 555
Henon M., 1972, In: Gravitational N-Body Problem. Ed. M. Lecar (Reidel: Dordrecht), p. 406
Jones B.F., Herbig G.H., 1979, AJ 84, 1872
Kiseleva L.G., Eggleton P.P., Anosova J.P., 1994a, MNRAS 267, 161
Kiseleva L.G., Eggleton P.P., Orlov V.V., 1994b, MNRAS 270, 936
Köhler R., Leinert C., 1998, A&A 331, 977
Kroupa P., Tout C.A., Gilmore G., 1991, MNRAS 251, 293
Kroupa P., 1995, MNRAS 277, 1522
Kroupa P., 1998, MNRAS 298, 231
Lada E.A., DePoy D.L., Evans N.J., Gatley I., 1991, ApJ 371, 171
Leinert, C., Zinnecker, H., Weitzel, N., Christou, J., Ridgway, S.T., Jameson, R., Haas, M., Lenzen, R., 1993, A&A, 278, 129
Leinert C., Henry T., Glindemann A., McCarthy D.W., 1997, A&A 325, 159
Magazzu, A., Martin, E.L., Sterzik, M.F. et al., 1997, A&AS 124, 449
Mathieu R., 1994, ARAA 32, 405
McAlister H.A., Mason B.D., Hartkopf W.I., Shara M.M., 1993, AJ 106, 1639
McDonald J.M., Clarke C.J., 1993, MNRAS 262, 800
McDonald J.M., Clarke C.J., 1995, MNRAS 275, 671
McMillan S.L.W., Hut P., 1996, ApJ 467, 348
Mikkola S., Aarseth S.J., 1990, Cel. Mech. Dyn. Astr. 47, 375
Mikkola S., Aarseth S.J., 1993, Cel. Mech. Dyn. Astr. 57, 439
Mikkola S., Valtonen M.J., 1986, MNRAS 223, 269
Miller G.E., Scalo J.M., 1979, ApJS 41, 513
Monaghan J.J., 1976a, MNRAS 176, 63
Monaghan J.J., 1976b, MNRAS 177, 583
Monaghan J.J., 1977, MNRAS 179, 31
Monaghan J.J., 1994, ApJ 420, 692
Monaghan J.J., Lattanzio J. C., 1991, ApJ 375, 177
Nash P.E., Monaghan J.J., 1978, MNRAS 184, 119
Neuhäuser R., Sterzik M.F., Torres G., Martin E.L., 1995, A&A 299, L13
Neuhäuser R., 1997, Science 276, 1363
Neuhäuser R., Torres G., Sterzik M.F., Randich S., 1997, A&A 325, 647
Neuhäuser R. et al., 1998, A&A 334, 873
Padgett D.L., Strom S.E., Ghez A., 1997, ApJ 477, 705
Petr M., Cdu Foresto V., Beckwith S.V.W., Richichi A., McCaughrean M.J., 1998, ApJ 500, 825
Prosser, C.F., Stauffer, J.R., Hartmann, L., Soderblom, D.R., Jones, B.F., Werner, M.W., McCaughrean, M.J., 1994, ApJ, 412, 517
Reipurth, B., Zinnecker, H., 1993, A&A 278, 89
Saslaw W.C., Valtonen M.J., Aarseth S.J., 1974, ApJ 190, 253
Soderblom D.R., King J.R., Henry T.J., 1998, AJ, in press
Standish E.M., 1972, A&A 21, 185
Sterzik M.F., Alcala J.M., Neuhäuser R., Schmitt J.H.M.M., 1995, A&A 297, 418
Sterzik M.F., Durisen R.H. (SD), 1995, A&A 304, L9
Sterzik M.F., Schmitt J.H.M.M., 1997, AJ 114, 1673
Sterzik M.F., Alcalá J.M., Neuhäuser R., Durisen R.H., 1998, In: The Orion Complex Revisited. Eds. A. Burkert & M. McCaughrean (ASP: San Francisco), in press
Szebehely V.G., 1972, AJ 77, 169
Terebey S., van Buren D., Padgett D.L., Hancock T., Brundage M., 1998, ApJL 506, in press
Tokovinin, A.A. 1997, A&AS 124, 75
Truelove J.K., Klein R.I., McKee C.F. et al., 1997, ApJL 489, L179
Truelove J.K., Klein R.I., McKee C.F. et al., 1998, ApJ 495, 821
Valtonen M. J., 1976, Ap&SS 42, 331
Valtonen M., Mikkola S., 1991, ARAA 29, 9
Valtonen M., 1997, ApJ 485, 785
Valtonen M., 1998, A&A 334, 169
van Albada T.S., 1968a, Bull. Astron. Inst. Neth. 19, 479
van Albada T.S., 1968b, Bull. Astron. Inst. Neth. 20, 57